Controlling Stationary One-Way Quantum Steering in Cavity Magnonics

Zhi-Bo Yang,[1,2] Xuan-De Liu,[1] Xin-Yi Yin,[1] Ying Ming,[2,*] Hong-Yu Liu,[2,†] and Rong-Can Yang[1,3,‡]

[1] *Fujian Provincial Key Laboratory of Quantum Manipulation and New Energy Materials, and College of Physics and Energy, Fujian Normal University, Fuzhou 350117, China*

[2] *Department of Physics, College of Science, Yanbian University, Yanji, Jilin 133002, China*

[3] *Fujian Provincial Collaborative Innovation Center for Optoelectronic Semiconductors and Efficient Devices, Xiamen 361005, China*

(Received 13 October 2020; revised 17 December 2020; accepted 25 January 2021; published 17 February 2021)

We show how to implement stationary one-way quantum steering with strong entanglement in a cavity magnonic system that consists of two magnon modes and a microwave cavity. The cavity is driven by a squeezed vacuum field generated by a flux-driven Josephson parameter amplifier and coupled to two Kittel modes via magnetic dipole interaction. We find that the steering directivity only depends on the ratio of two coupling rates (i.e., the ratio of coherent information exchange frequencies) and is barely affected by the dissipation of the system. Meanwhile, the entanglement and steering can be significantly enhanced due to the squeezed vacuum field and thus are more robust against thermal noises. This provides an active method to manipulate the steering directivity instead of adding asymmetric losses or noises to subsystems at the cost of reducing steerability.

DOI: 10.1103/PhysRevApplied.15.024042

I. INTRODUCTION

In 1935, Einstein, Podolsky, and Rosen (EPR) presented a famous argument against the completeness of quantum mechanics [1]. Since then, many researchers have argued whether quantum mechanics is complete. To solve this problem, Schrödinger introduced the term "entanglement" to discuss the EPR paradox that implies the existence of steering [2,3]. Quantum steering, as a strict subset of entanglement, refers to the nonclassical correlations in a bipartite scenario (say Alice and Bob) in which one of the parties (say Alice) can deduce the state that the other distant one holds according to her local measurement outcomes applied on the part of the entangled state in her side. Quantum steering may be achieved in various systems such as optomechanical systems [4–8], atom-mechanical systems [9,10], antiferromagnetic (AFM) systems [11], etc. And it can be applied to quantum key distribution [12–14], quantum secret sharing [15–17], one-way quantum computing [18], quantum teleportation [19–21], subchannel discrimination [22], etc. However, in practice, achieving one-way quantum steering with strong entanglement and flexible controllability remains a demanding issue, especially in the situation of lack of experimental resources.

In recent years, ferrimagnetic (FiM) materials, especially yttrium-iron-garnet (YIG) spheres, have attracted great interest due to their high spin density and low damping rate. The hybrid quantum system containing magnons is different from traditional optomechanical systems [23]. The Kittel mode [24], a spatially uniform mode of the FiM spin waves in a YIG sphere, can strongly couple to the microwave photons, called cavity-magnon polaritons [25–29]. In addition, the Kittel mode can also couple with a variety of different systems [30–47], no matter continuous-variable or discrete-variable systems. The coherent interaction between microwave photons and spin waves is a key ingredient for the development of complex hybrid systems and also a current focus of research. Indeed, quanta of excitation of the spin wave modes, called magnons, can also interact coherently with microwave photons and optical photons in the fields of cavity magnonics and cavity optomagnonics, respectively. Cavity magnonics is an emerging field that studies magnons strongly coupled to microwave photons via the magnetic dipole interaction [48,49]. Many interesting phenomena are observed in cavity magnonics, such as exceptional point [30], remote manipulation of spin current [31], bistability [32], cavity-mediated magnon long-range coupling [47], etc. However, cavity optomagnonics [48,50] mainly explores the hybrid system in which light and magnons are coupled through the magneto-optical effect, where the interaction between optical photons and spin waves in FiM crystals is indirect,

*mingying@ybu.edu.cn
†liuhongyu@ybu.edu.cn
‡rcyang@fjnu.edu.cn

which is similar to the interaction between magnetostatic modes and superconducting qubits [33]. Thus, there are also many notable physical phenomena revealed in cavity optomagnonics, such as optical probe spin wave physics [51–53], the observation of Bose-Einstein condensation in YIG thin films [54,55], optical whispering-gallery modes in YIG spheres [36,56], etc. In this article, we focus on a cavity magnonic system that consists of a microwave cavity and two YIG spheres. In fact, based on similar systems, many interesting results are revealed in cavity magnonics, such as Kerr-effect-induced magnon entanglement [43], dissipative magnon-photon coupling [45,47], long-distance YIG sphere coupling [57], higher-order exceptional point [58], etc.

Here we use a full quantum theory of the cavity magnonic system to prove that it is possible to implement a controllable one-way steering with strong entanglement, wherein "controllable" refers to that we can implement $1 \rightarrow 2$ one-way steering, $2 \rightarrow 1$ one-way steering, or $1 \rightleftharpoons 2$ two-way steering with different parameter mechanisms. The steering directivity only depends on the ratio of two cavity-magnon coupling rates rather than the dissipations of the system. The generated entanglement and steering are robust against temperature, and can be enhanced by increasing the squeezing parameter. We also show that squeezed vacuum field driving is significant for the implementation of one-way steering with strong entanglement by using experimentally feasible parameters. The magnon-magnon entanglement and steering arise from the squeezed field within the system and the steering directivity can be manipulated by adjusting the position of YIG spheres in the cavity. Therefore, our scheme may have potential applications for quantum information science.

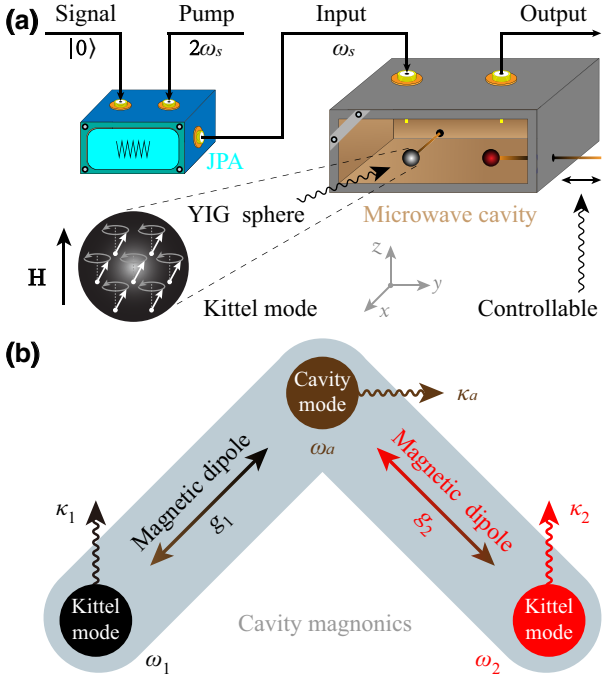

FIG. 1. (a) Sketch of the cavity magnonic system. Two magnon modes in two YIG spheres are placed inside a microwave cavity. The cavity field is driven by a weak squeezed vacuum field generated by a flux-driven Josephson parametric amplifier. The bias magnetic field for producing the Kittel mode is along the z axis whereas the magnetic field of the cavity mode is along the $\pm y$ axis. (b) Two Kittel modes are, respectively, coupled to the microwave cavity mode with coupling rates g_1 and g_2 via the magnetic dipole interaction. The microwave cavity mode and two magnon modes have dissipation rates κ_a, κ_1, and κ_2, respectively. See text for more details.

II. MODEL

A hybrid system is considered with cavity magnonics depicted schematically in Fig. 1(a), which is composed of two identical YIG spheres and a three-dimensional (3D) microwave cavity. Two Kittel modes couple directly to a common microwave cavity mode through magnetic dipole interaction shown in Fig. 1(b). We assume that the size of the two spheres is much smaller than the microwave wavelength, so that the effect of radiation pressure acting on the two spheres can be ignored [39,40,42,46]. The Hamiltonian for the whole system is [59]

$$\mathcal{H}/\hbar = \omega_a a^\dagger a + \sum_{j=1}^{2}\left[\omega_j m_j^\dagger m_j + g_j (m_j^\dagger a + m_j a^\dagger)\right], \quad (1)$$

where $a^\dagger$ and $m_j^\dagger$ (a and m_j) are, respectively, the creation (annihilation) operators of the cavity mode with frequency ω_a and the jth magnon mode with frequency ω_j and satisfy standard commutation relations for bosons.

In addition, the frequency of the jth magnon mode ω_j can be adjusted in a large range by altering the bias magnetic field $\mathbf{H}$ in the z direction with amplitude H_z via $\omega_j = \gamma_0 H_z$, where $\gamma_0/2\pi = 2.76$ MHz/Oe is the gyromagnetic ratio. The parameter g_j denotes the cavity-jth-magnon coupling rate that can be modulated by varying the direction of the bias field or the position of the YIG spheres inside the microwave cavity [35]. Furthermore, the cavity mode is driven by a weak squeezed vacuum field (with driving frequency ω_s) generated by a flux-driven Josephson parametric amplifier (JPA) with a pump field at frequency $2\omega_s$ and vacuum fluctuations at the signal input port [60–72]. In this case, quantum Langevin equations for the system can be given by

$$\begin{aligned} \dot{a} &= -(i\Delta_a + \kappa_a)a - i\sum_{j=1}^{2} g_j m_j + \sqrt{2\kappa_a}a^{\text{in}}, \\ \dot{m}_j &= -(i\Delta_j + \kappa_j)m_j - ig_j a + \sqrt{2\kappa_j}m_j^{\text{in}}, \end{aligned} \quad (2)$$

where $\Delta_a = \omega_a - \omega_s$ and $\Delta_j = \omega_j - \omega_s$. κ_a and κ_j ($a^{\rm in}$ and $m_j^{\rm in}$) are, respectively, the dissipation rates (input noise operators) of the cavity mode and the jth magnon mode. In this article, the JPA is used to shape the noise properties of quantum fluctuations of the cavity field, leading to a squeezed cavity field. Thus, the input noise operators are zero mean and characterized by the following correlation functions [73]: $\langle a^{\rm in\dagger}(t)a^{\rm in}(t')\rangle = N\delta(t-t')$, $\langle a^{\rm in}(t)a^{\rm in\dagger}(t')\rangle = (N+1)\delta(t-t')$, $\langle a^{\rm in}(t)a^{\rm in}(t')\rangle = M\delta(t-t')$, $\langle a^{\rm in\dagger}(t)a^{\rm in\dagger}(t')\rangle = M^*\delta(t-t')$, $\langle m_j^{\rm in\dagger}(t)m_j^{\rm in}(t')\rangle = n_j\delta(t-t')$, and $\langle m_j^{\rm in}(t)m_j^{\rm in\dagger}(t')\rangle = (n_j+1)\delta(t-t')$, where $N = (n_a+1)\sinh^2 r + n_a\cosh^2 r$, $M = (2n_a+1)e^{i\theta}\sinh r\cosh r$, and $n_o = [\exp(\hbar\omega_o/k_BT)-1]^{-1}$, $(o = a,j)$ with r being the squeezing parameter and θ the phase of the squeezed vacuum field.

III. ENTANGLEMENT AND STEERING

To quantify the entanglement and steering between the two Kittel modes, we introduce three sets of quadrature components, $X_a^{(\rm in)}, Y_a^{(\rm in)}, X_1^{(\rm in)}, Y_1^{(\rm in)}, X_2^{(\rm in)}, Y_2^{(\rm in)}$, which are defined as $X_a^{(\rm in)} = (a^{(\rm in)} + a^{(\rm in)\dagger})/\sqrt{2}$, $Y_a^{(\rm in)} = (a^{(\rm in)} - a^{(\rm in)\dagger})/\sqrt{2}i$, $X_j^{(\rm in)} = (m_j^{(\rm in)} + m_j^{(\rm in)\dagger})/\sqrt{2}$, and $Y_j^{(\rm in)} = (m_j^{(\rm in)} - m_j^{(\rm in)\dagger})/\sqrt{2}i$. Then, the linearized Langevin equations can be written in the matrix form

$$\dot{\sigma}(t) = \mathcal{A}\sigma(t) + \varrho(t) \tag{3}$$

with $\sigma(t) = [X_a(t), Y_a(t), X_1(t), Y_1(t), X_2(t), Y_2(t)]^T$ and $\varrho(t) = [\sqrt{2\kappa_a}X_a^{\rm in}(t), \sqrt{2\kappa_a}Y_a^{\rm in}(t), \sqrt{2\kappa_1}X_1^{\rm in}(t), \sqrt{2\kappa_1}Y_1^{\rm in}(t), \sqrt{2\kappa_2}X_2^{\rm in}(t), \sqrt{2\kappa_2}Y_2^{\rm in}(t)]^T$ being the vectors for quantum fluctuations and noises, respectively. The drift matrix $\mathcal{A}$ reads

$$\mathcal{A} = \begin{bmatrix} -\kappa_a & \Delta_a & 0 & g_1 & 0 & g_2 \\ -\Delta_a & -\kappa_a & -g_1 & 0 & -g_2 & 0 \\ 0 & g_1 & -\kappa_1 & \Delta_1 & 0 & 0 \\ -g_1 & 0 & -\Delta_1 & -\kappa_1 & 0 & 0 \\ 0 & g_2 & 0 & 0 & -\kappa_2 & \Delta_2 \\ -g_2 & 0 & 0 & 0 & -\Delta_2 & -\kappa_2 \end{bmatrix}. \tag{4}$$

Because of the linearity of the Langevin equations and the Gaussian nature of the quantum noises, the system will decay to a stationary Gaussian state that can be completely characterized by a 6×6 covariance matrix (CM) $\mathcal{V}$ in phase space: $\mathcal{V}_{ij} = \langle\sigma_i(t)\sigma_j(t') + \sigma_j(t')\sigma_i(t)\rangle/2$, $(i,j = 1,2,\ldots,6)$. The steady-state CM $\mathcal{V}$ can be obtained straightforwardly by solving the Lyapunov equation [74]

$$\mathcal{A}\mathcal{V} + \mathcal{V}\mathcal{A}^T = -\mathcal{D} \tag{5}$$

with $\mathcal{D} = \mathcal{D}_a \bigoplus \mathcal{D}_m$. Here [59]

$$\mathcal{D}_a = \begin{bmatrix} \kappa^+ & \kappa^a \\ \kappa^a & \kappa^- \end{bmatrix}, \quad \mathcal{D}_m = \begin{bmatrix} \kappa_1^m & 0 & 0 & 0 \\ 0 & \kappa_1^m & 0 & 0 \\ 0 & 0 & \kappa_2^m & 0 \\ 0 & 0 & 0 & \kappa_2^m \end{bmatrix} \tag{6}$$

with $\kappa^+ = \kappa_a(2N+1+M+M^*)$, $\kappa^- = \kappa_a(2N+1-M-M^*)$, $\kappa^a = i\kappa_a(M^*-M)$, and $\kappa_j^m = \kappa_j(2n_j+1)$. It is noted that Eq. (6) is defined through $\mathcal{D}_{ij}\delta(t-t') = \langle\varrho_i(t)\varrho_j(t') + \varrho_j(t')\varrho_i(t)\rangle/2$.

For the continuous-variable two-mode Gaussian state of two magnon modes, a computable criterion of quantum steering based on quantum coherent information has been introduced [75]. While for quantum entanglement, it is convenient to use the logarithmic negativity E_N to quantify its level [76–79]. It is noted that all the above-mentioned measures can be computed from the reduced 4×4 CM $\mathcal{V}_m$ for the two magnon modes:

$$\mathcal{V}_m = \begin{bmatrix} \mathcal{V}_1 & \mathcal{V}_3 \\ \mathcal{V}_3^T & \mathcal{V}_2 \end{bmatrix}, \tag{7}$$

where $\mathcal{V}_1$, $\mathcal{V}_2$, and $\mathcal{V}_3$ are 2×2 sub-block matrices of $\mathcal{V}_m$. In this case, the logarithmic negativity for the two magnon modes is expressed as

$$E_N = \max[0, -\ln(2\nu)], \tag{8}$$

where $\nu = \sqrt{\mathcal{E} - (\mathcal{E}^2 - 4\mathcal{R})^{1/2}}/\sqrt{2}$ and $\mathcal{E} = \mathcal{R}_1 + \mathcal{R}_2 - 2\mathcal{R}_3$, with $\mathcal{R}_1 = \det\mathcal{V}_1$, $\mathcal{R}_2 = \det\mathcal{V}_2$, $\mathcal{R}_3 = \det\mathcal{V}_3$, and $\mathcal{R} = \det\mathcal{V}_m$ being symplectic invariants. Moreover, the Gaussian quantum steering is given by

$$\mathcal{G}_{1\to 2} = \max\left[0, \frac{1}{2}\ln\frac{\mathcal{R}_1}{4\mathcal{R}}\right],$$
$$\mathcal{G}_{2\to 1} = \max\left[0, \frac{1}{2}\ln\frac{\mathcal{R}_2}{4\mathcal{R}}\right]. \tag{9}$$

In order to check the asymmetric steerability of the two-mode Gaussian state, we introduce the steering asymmetry defined as [80]

$$\mathcal{G} = |\mathcal{G}_{1\to 2} - \mathcal{G}_{2\to 1}|. \tag{10}$$

IV. NUMERICAL RESULTS AND ANALYSIS

The foremost task of studying properties of the entanglement and steering in such a cavity magnonic system is to find optimal detunings Δ_a, Δ_1, and Δ_2, i.e., optimal effective interactions between magnon modes that can generate entanglement and steering. The related density plots are shown in Fig. 2 with the magnon-magnon entanglement E_N and symmetric steering (the $1\to 2$

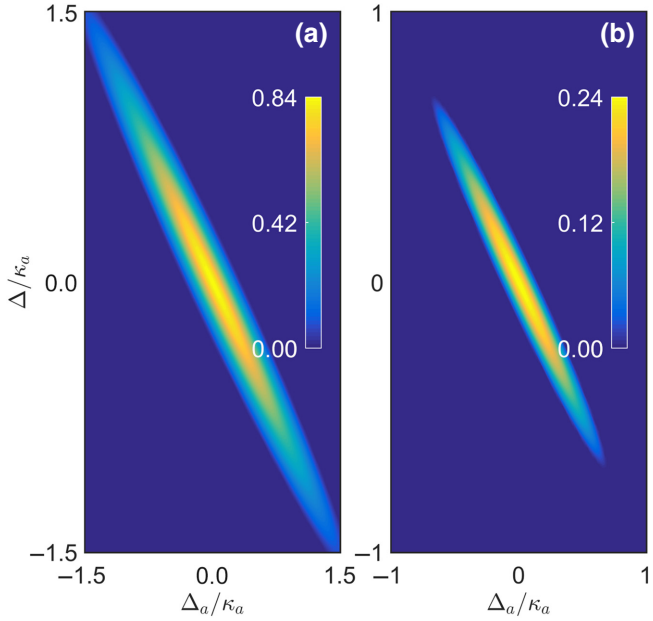

FIG. 2. (a) The entanglement E_N and (b) steering ($\mathcal{G}_{1\to2} = \mathcal{G}_{2\to1}$) versus Δ_a and Δ. We have chosen $\omega_{a,1,2}/2\pi = 10$ GHz, $\kappa_a/2\pi = 5\kappa_{1,2}/2\pi = 5$ MHz, $g_{1,2} = 4\kappa_a$, $r = 2$, $\theta = 0$, and $T = 20$ mK.

steering $\mathcal{G}_{1\to2}$ and the $2 \to 1$ steering $\mathcal{G}_{2\to1}$) as functions of the frequency detunings, where the following experimentally feasible parameters are utilized [30,35]: $\omega_{a,1,2}/2\pi = 10$ GHz, $\kappa_a/2\pi = 5\kappa_{1,2}/2\pi = 5$ MHz, $g_{1,2} =$

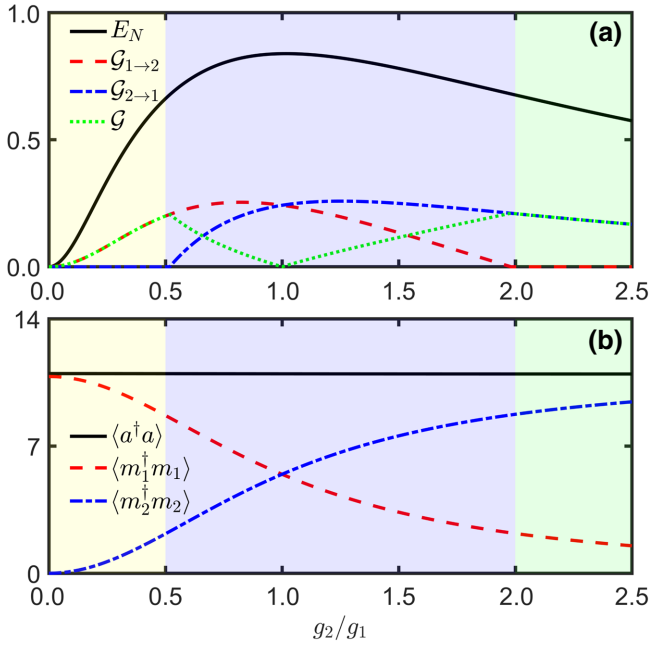

FIG. 3. (a) The entanglement E_N and steering ($\mathcal{G}_{1\to2}$ and $\mathcal{G}_{2\to1}$) and (b) populations of modes versus g_2/g_1 for a fixed g_1. We have chosen $\Delta_a = \Delta = 0$, and other parameters are the same as those in Fig. 2.

$4\kappa_a$, and a low temperature $T = 20$ mK. In addition, two 250-μm-diameter YIG spheres are used and their spin numbers are both about $N_{\rm YIG} \simeq 3.5 \times 10^{16}$. For the sake of simplicity, we assume the two YIG spheres are magnetized by a common bias magnetic field, such that they share the same frequency $\omega_{1,2} = \gamma_0 H_z$, i.e., $\omega_1 = \omega_2$ and $\Delta_1 = \Delta_2 = \Delta$. All results are in the steady state guaranteed by the negative eigenvalues (real parts) of the drift matrix $\mathcal{A}$ [59,81]. Figure 2 shows that $\Delta_a = \Delta = 0$ (i.e., $\omega_a = \omega_{1,2} = \omega_s$) is optimal for entanglement and steering. At the resonant frequency, we observe the maximum amount of entanglement and steering. Note that we have set $g_1 = g_2 = 4\kappa_a$ in Fig. 2(b) to allow system symmetry such that they are the same for the $1 \to 2$ steering $\mathcal{G}_{1\to2}$ and the $2 \to 1$ steering $\mathcal{G}_{2\to1}$.

In the following, our aim is to obtain a controllable one-way quantum steering in the strong cavity-magnon interaction rates. To demonstrate the idea, we plot in Fig. 3(a) the entanglement E_N and steering ($\mathcal{G}_{1\to2}$ and $\mathcal{G}_{2\to1}$) and in Fig. 3(b) the populations of modes versus the ratio of couplings g_2/g_1 for a fixed g_1, where $\Delta_a = \Delta = 0$ and the other parameters are the same as the previous ones shown in Fig. 2. From Fig. 3(a), we see that E_N first increases and then slowly decreases with an increase of g_2/g_1. It reaches its maximum value when $g_2 = g_1$. The steering from the first magnon mode to the second one $\mathcal{G}_{1\to2}$ has a similar property to E_N: it decreases to and then remains zero when $g_2/g_1 \geq 2$. On the contrary, the steering from the second magnon mode to the first one $\mathcal{G}_{2\to1}$ first remains zero when $g_2/g_1 \leq 1/2$, and then has a similar property to E_N. These results tell us that $1 \to 2$ ($2 \to 1$) one-way steering $\mathcal{G}_{1\to2}$ ($\mathcal{G}_{2\to1}$) can be implemented with $g_2/g_1 \leq 1/2$ ($g_2/g_1 \geq 2$). Otherwise, when the ratio satisfies $1/2 < g_2/g_1 < 2$, two-way steering occurs. Therefore, when certain conditions are met, there exist entangled states that are $1 \to 2$ ($2 \to 1$) one-way steerable. The $1 \to 2$ one-way steering implies that Alice can convince Bob that their shared state is entangled, while the converse is not true [80]. The most obvious application is that it provides security in one-sided device-independent quantum key distribution, where the measurement apparatus of one party only is untrusted. The result comes from the fact that the magnon mode with larger population is more difficult to steer by the other one [see Fig. 3(b)]. Interestingly, when $g_2/g_1 = 1$, we have $\mathcal{G}_{1\to2} = \mathcal{G}_{2\to1}$ and the entanglement $E_N = \max[E_N]$. Thus, the asymmetric steering is carried out at the cost of a decrease of the entanglement of the system. Our scheme shows one advantage: the system creates one-way steering without imposing additional conditions of asymmetric losses or noises in the subsystems, but changes the population of the two magnon modes through the ratio of coherent information exchange frequencies. In order to show the steering directivity clearly, we use the pink area to represent the presence of no-way steering, the yellow and green areas to separately depict the presence of one-way steering

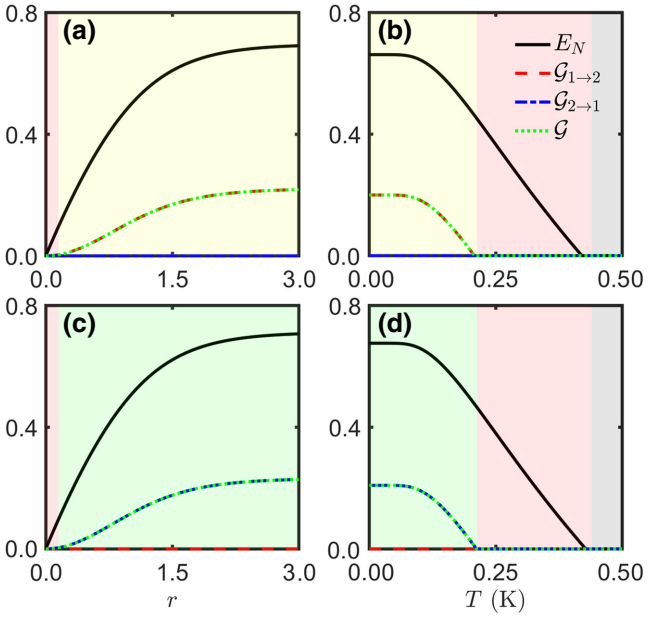

FIG. 4. The entanglement E_N and steering ($\mathcal{G}_{1\to2}$ and $\mathcal{G}_{2\to1}$) versus (a),(c) r and (b),(d) T. We have chosen $g_2 = 2\kappa_a$ in (a),(b), $g_2 = 8\kappa_a$ in (c),(d), and the other parameters are the same as those in Fig. 3.

for $1 \to 2$ and $2 \to 1$, and the blue area to demonstrate the presence of $1 \rightleftharpoons 2$ two-way steering. The gray area represents the presence of no entanglement, and $\mathcal{G} \neq 0$ stands for asymmetry of steering. Note that similar rules are suitable for the rest passages.

Besides the ratio of two coupling rates between the magnon modes and cavity mode, let us continue by illustrating the influence of the squeezing parameter r and environment temperature T, which is shown in Fig. 4, with the entanglement E_N and steering ($\mathcal{G}_{1\to2}$ and $\mathcal{G}_{2\to1}$) as functions of r and T for $g_2 = 2\kappa_a$ and $g_2 = 8\kappa_a$. The other parameters are the same as those in Fig. 3. We observe that E_N and $\mathcal{G}_{1\to2}$ ($\mathcal{G}_{2\to1}$) increase with an increase of r in Fig. 4(a) [Fig. 4(c)] and they are fairly robust against temperature when $T \lesssim 0.1$ K, which is shown in Fig. 4(b) [Fig. 4(d)], while the steering on the other side is blocked. The result means that the squeezing rate of the cavity mode can increase the level of steering to some extent, but it cannot change the steering directivity. Similarly, the thermal noises induced by environment temperature also cannot affect the steering directivity, but it may deteriorate the steerability and entanglement. Moreover, the steerability is more sensitive to the environment temperature than the entanglement. For example, the one-way steering ($\mathcal{G}_{1\to2}$ or $\mathcal{G}_{2\to1}$) disappears at $T \simeq 0.21$ K, while the entanglement E_N decreases to zero until $T \simeq 0.44$ K.

In order to explore the upper-limit temperature at which the present scheme can work, we further study the effect of the critical temperature with some other parameters relaxed, such as resonance frequencies and dissipative rates. At first, the temperature-dependent behavior of a cavity-magnon polarization is experimentally revealed in a recent article, where the cavity-magnon polarization can occur at a temperature from 0.03 to 290 K [82]. The main factor affecting the cavity-magnon coupling rates $g_{1,2}$ is the saturation magnetization, which is dependent on temperature according to Bloch's $T^{3/2}$ law when $T \geq 100$ K [83]. While for $T < 100$ K, the behavior of coupling rates $g_{1,2}$ is different. Additional anti-crossings of much smaller coupling rate appear at lower values of the applied external field but still rather close to the resonance field of the Kittel mode [82]. In addition, the other parameters are hardly affected by temperature (e.g., $\omega_{a,1,2}$ and $\kappa_{a,1,2}$) so that their effect can be ignored. Although strong cavity-magnon coupling rates can be achieved at high temperatures, we can see from Figs. 4(b) and 4(d) that the entanglement (steering) only exists at $T \lesssim 0.44$ (0.21) K if we maintain the resonance frequencies to be only below 10 GHz. Taking this into account, if we increase the resonance frequencies of the two magnon modes to $\omega_{1,2}/2\pi = 90, 250, 600$ GHz and a microwave cavity (squeezed pump field) matching two resonance frequencies, the critical temperature of entanglement (steering) will be expanded to $T \simeq 4.7$, 13, 31.3 (2, 5.7, 13.6) K. In fact, the resonance frequency of magnons in the YIG sphere is only related to the amplitude H_z of the bias field [84]. Magnon modes with frequencies $\omega_{1,2}/2\pi = 90, 250, 600$ GHz need a bias field with amplitude $H_z \simeq 3.26 \times 10^4, 9.06 \times 10^4, 2.17 \times 10^5$ Oe to magnetize two YIG spheres to saturation. Nevertheless, due to the high cost of the realization of an ultrastrong bias magnetic field, the resonance frequency of magnon modes in most current experiments is generally of the order of tens of gigahertz. Additionally, reducing the dissipation rates of the cavity and magnon modes can also effectively increase the critical temperature [46]. In Fig. 5, we show the entanglement and steering as functions of T and κ, where $\kappa_{1,2} = \kappa$ and $\kappa_a = 5\kappa$. From the trend of the contour lines in the figure, we can observe that the changes of the resonance frequencies and dissipation rates of the cavity and magnon modes have a very large impact on the critical temperature to let our present scheme work at higher temperature. If the resonance frequencies can be increased to several hundred gigahertz, then the present protocol may work at a temperature of tens of kelvins. Of course, we should admit that a high frequency has not been used in the current experiment using YIG spheres or other FiM materials. Fortunately, we note that some other researchers have utilized AFM materials that can work at a frequency of a few terahertz. We hope that our proposal may be realized in the AFM-cavity system [11].

Finally, we investigate the effect of individual magnon mode dissipation rate on the entanglement and steering, which is shown in Fig. 6 with the entanglement E_N and steering ($\mathcal{G}_{1\to2}$ and $\mathcal{G}_{2\to1}$) as functions of the dissipation

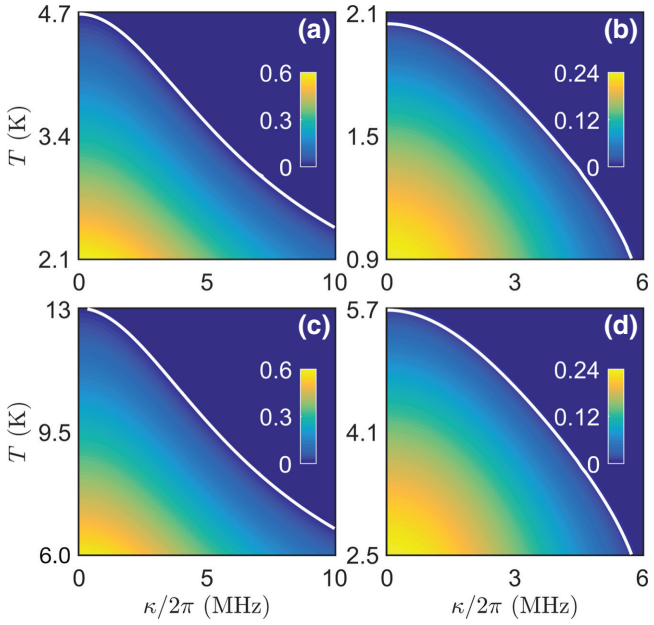

FIG. 5. (a),(c) The entanglement E_N and (b),(d) steering ($\mathcal{G}_{1\to2} = \mathcal{G}_{2\to1}$) versus κ and T. We have chosen $r = 2$, $\theta = 0$, $\kappa_{1,2} = \kappa$, $\kappa_a = 5\kappa$, $g_{1,2}/2\pi = 20$ MHz, and $\omega_{a,1,2}/2\pi = 90$ GHz in (a),(b) and $\omega_{a,1,2}/2\pi = 250$ GHz in (c),(d).

rates of the two magnon modes for $g_2 = 3\kappa_a$ and $g_2 = 6\kappa_a$. The other parameters are chosen to be the same as those in Fig. 3. The figure shows that an increase of $\kappa_{1,2}$ has a negative effect on the entanglement and steering. In addition, no matter which directivity of the steering we would like to control, the increase of $\kappa_{1,2}$ can only deteriorate the entanglement and steering level, although it cannot change the steering directivity.

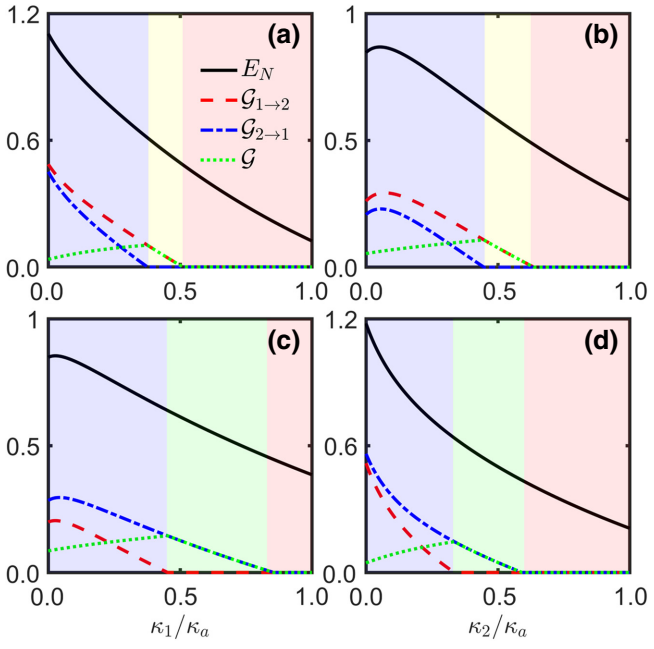

FIG. 6. The entanglement E_N and steering ($\mathcal{G}_{1\to2}$ and $\mathcal{G}_{2\to1}$) versus (a),(c) κ_1/κ_a and (b),(d) κ_2/κ_a for fixed κ_a. We have chosen $g_2 = 3\kappa_a$ in (a),(b) and $g_2 = 6\kappa_a$ in (c),(d). The other parameters are the same as in Fig. 3.

V. EXPERIMENTAL IMPLEMENTATION

Let us discuss the feasibility of the present configuration. It contains two undoped single-crystal YIG spheres and a 3D rectangular cavity. The reason for using spherical samples is to avoid the effect of an inhomogeneous demagnetization field. In addition, to suppress the interaction of the YIG spheres with other magnetostatic modes, we utilize a nearly uniform microwave field in a large cavity with cavity volume being $4.4 \times 2 \times 0.6$ cm^3 [30]. The cavity can be made of high-conductivity copper with TE_{120} at $\omega_a/2\pi \simeq 10$ GHz and its internal dissipation is about $\kappa_{\mathrm{in}}/2\pi \simeq 1$ MHz at low temperature $T \simeq 20$ mK, which can be implemented using a dilution refrigerator (or using a ^{4}He continuous-flow cryostat [82]). Taking into account external dissipation of the cavity κ_{ex}, which arises from the port connected to the JPA, we assume the total dissipation of the microwave cavity to be $\kappa_a = \kappa_{\mathrm{in}} + \kappa_{\mathrm{ex}} \simeq 2\pi \times 5$ MHz (corresponding to cavity quality factor $\mathcal{Q}_a = \omega_a/\kappa_a \simeq 2 \times 10^3$). The dissipation rates of the two YIG spheres, which come from the surface roughness as well as the impurities or defects of the YIG spheres, are chosen to be $\kappa_{1,2}/2\pi \simeq 1$ MHz [26,85]. Additionally, the two YIG spheres are both magnetized to saturation by a common bias magnetic field with amplitude $H_z \simeq 3.62 \times 10^3$ Oe (corresponding to the resonance frequencies of the magnon modes $\omega_{1,2}/2\pi \simeq 10$ GHz).

Due to the high spin density of the YIG spheres and few excitations of magnons, the present system can be described by the Hamiltonian represented in Eq. (1) and a strong coherent coupling mechanism ($g_{1,2} > \kappa_{a,1,2}$) can easily be achieved [25–29], which can be reflected by the reflection spectrum under continuous driving of the microwave cavity. In this case, we can get the relation between cavity-magnon coupling rates and the location of YIG spheres [30,86]. In order to change the coupling rates, we can move the position of the YIG spheres to obtain different ratios between the two magnon-cavity coupling rates. For example, the first YIG sphere can be fixed at the 1/4 (3/4)-length position away from the left-hand side of the first normalized microwave magnetic field of the cavity TE_{120} mode, while the second one glued on a wooden rod is inserted into the cavity through a hole to adjust its location along the y direction using a displacement platform [see Fig. 1(a) or the device structure in Ref. [30]]. For the sake of clarity, we illustrate the intensity and direction of the magnetic field distribution of the cavity TE_{120} mode and the position of the two YIG spheres in Fig. 7.

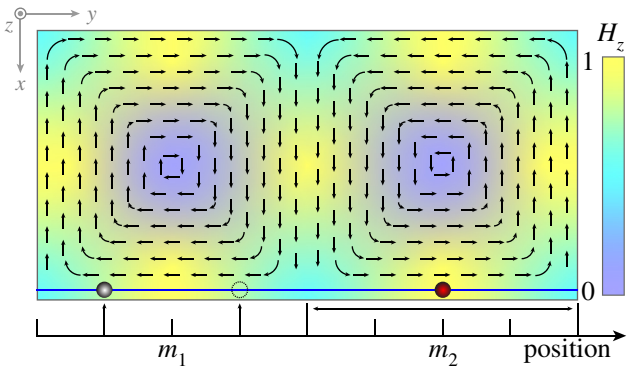

FIG. 7. The intensity and direction of magnetic field distribution of the cavity TE_{120} mode and the position of two YIG spheres (top view).

Finally, the generated entanglement or steering can be verified by measuring the corresponding CMs [73,87], in which the state of the magnon mode can be determined by sending a weak microwave probe field and measuring with homodyne detection. This requires the dissipation rate of the cavity mode to be much larger than that of the two magnon modes (i.e., $\kappa_a \gg \kappa_1 = \kappa_2 > 0$) and the two cavity-magnon coupling rates be unequal [e.g., $g_2 = 2g_1 > 0$ in order for $\langle m_2^\dagger m_2\rangle \gg \langle m_1^\dagger m_1\rangle > 0$; see Fig. 3(b)]. In this case, even if all cavity photons and magnons (the first magnon mode) decay, magnons (the second magnon mode) remain almost unchanged when the driving field is switched off but a probe field is sent to the cavity.

VI. CONCLUSION AND OUTLOOK

In summary, we have presented a scheme to obtain a controllable one (two)-way quantum steering with strong entanglement, which can be modulated by the ratio of coherent information exchange frequencies between two Kittel modes and the cavity mode based on experimentally feasible parameters. Instead of introducing different amounts of losses or noises to subsystems, our scheme provides inspiration for manipulating the asymmetric quantum steering with enhanced steerability via a JPA. The entanglement and steering are quite robust against temperature. Therefore, one-way steering may be realized in cavity magnonic systems and it may have important applications in quantum key distribution, quantum secret sharing, one-way quantum computing, quantum teleportation, subchannel discrimination, etc.

Finally, let us make a brief outlook and discuss some related issues. Our present scheme is realized with two YIG spheres coupled to a microwave cavity and may be limited by the resonance frequency only to tens of gigahertz. But it is still very significant to utilize this configuration because it can easily be coupled to circuit quantum electrodynamic systems that are now candidates for quantum computers. Additionally, due to the ultralow magnetic damping of YIG, magnons may be considered as high-quality (high-$\mathcal{Q}_{1,2}$) memories with $\mathcal{Q}_{1,2} = \omega_{1,2}/\kappa_{1,2}$, which describes the ratio between the stored and per-cycle-dissipated amount of energy [88]. Furthermore, our idea may be extended to other similar systems with higher resonance frequencies, for example cavity optomagnonics via magneto-optical effect [89,90] and cavity spintronics with spins driven by femtosecond laser pulses [91]. The use of THz emission spectroscopy and spin-orbit interaction provides an idea for the realization of quantum steering in higher-frequency bands. Moreover, with the rapid development of THz spintronics and all-optical spin manipulation, this idea may be used for ultrafast magnetic control [92], i.e., THz spintronic devices. We expect that the present idea may provide an inspiration for quantum control.

ACKNOWLEDGMENTS

This work is supported by the Fujian Natural Science Foundation (Grants No. 2018J01661 and No. 2019J01431) and the Science and Technology project of Jilin Provincial Education Department of China during the 13th Five-Year Plan Period (Grant No. JJKH20200510KJ). We thank J.-M. Zhang and A.-D. Zhu for helpful suggestions.

[1] A. Einstein, B. Podolsky, and N. Rosen, Can quantum-mechanical description of physical reality be considered complete? Phys. Rev. **47**, 777 (1935).
[2] E. Schrödinger, Discussion of probability relations between separated systems, Proc. Camb. Philos. Soc. **31**, 555 (1935).
[3] E. Schrödinger, Probability relations between separated systems, Proc. Camb. Philos. Soc. **32**, 446 (1936).
[4] Q. Y. He and M. D. Reid, Einstein–Podolsky–Rosen paradox and quantum steering in pulsed optomechanics, Phys. Rev. A **88**, 052121 (2013).
[5] S. Kiesewetter, Q. Y. He, P. D. Drummond, and M. D. Reid, Scalable quantum simulation of pulsed entanglement and Einstein–Podolsky–Rosen steering in optomechanics, Phys. Rev. A **90**, 043805 (2014).
[6] H. Tan, X. Zhang, and G. Li, Steady-state one-way Einstein–Podolsky–Rosen steering in optomechanical interfaces, Phys. Rev. A **91**, 032121 (2015).
[7] R. Schnabel, Einstein–Podolsky–Rosen-entangled motion of two massive objects, Phys. Rev. A **92**, 012126 (2015).
[8] H. Tan, W. Deng, Q. Wu, and G. Li, Steady-state light-mechanical quantum steerable correlations in cavity optomechanics, Phys. Rev. A **95**, 053842 (2017).
[9] Q. Y. He and Z. Ficek, Einstein–Podolsky–Rosen paradox and quantum steering in a three-mode optomechanical system, Phys. Rev. A **89**, 022332 (2014).
[10] H. Tan and L. Sun, Hybrid Einstein–Podolsky–Rosen steering in an atom-optomechanical system, Phys. Rev. A **92**, 063812 (2015).
[11] S. S. Zheng, F. X. Sun, H. Y. Yuan, Z. Ficek, Q. H. Gong, and Q. Y. He, Enhanced entanglement and asymmetric EPR

steering between magnons, Sci. China-Phys. Mech. Astron. **64**, 210311 (2020).
[12] C. Branciard, E. G. Cavalcanti, S. P. Walborn, V. Scarani, and H. M. Wiseman, One-sided device-independent quantum key distribution: Security, feasibility, and the connection with steering, Phys. Rev. A **85**, 010301(R) (2012).
[13] T. Gehring, V. Händchen, J. Duhme, F. Furrer, T. Franz, C. Pacher, R. F. Werner, and R. Schnabel, Implementation of continuous-variable quantum key distribution with composable and one-sided-device-independent security against coherent attacks, Nat. Commun. **6**, 8795 (2015).
[14] N. Walk, S. Hosseni, J. Geng, O. Thearle, J. Y. Haw, S. Armstrong, S. M. Assad, J. Janousek, T. C. Ralph, T. Symul, H. M. Wiseman, and P. K. Lam, Experimental demonstration of Gaussian protocols for one-sided device-independent quantum key distribution, Optica **3**, 634 (2016).
[15] S. Armstrong, M. Wang, R. Y. Teh, Q. H. Gong, Q. Y. He, J. Janousek, H. A. Bachor, M. D. Reid, and P. K. Lam, Multipartite Einstein–Podolsky–Rosen steering and genuine tripartite entanglement with optical networks, Nat. Phys. **11**, 167 (2015).
[16] Y. Xiang, I. Kogias, G. Adesso, and Q. Y. He, Multipartite Gaussian steering: Monogamy constraints and quantum cryptography applications, Phys. Rev. A **95**, 010101(R) (2017).
[17] I. Kogias, Y. Xiang, Q. Y. He, and G. Adesso, Unconditional security of entanglement-based continuous-variable quantum secret sharing, Phys. Rev. A **95**, 012315 (2017).
[18] C. M. Li, K. Chen, Y. N. Chen, Q. Zhang, Y. A. Chen, and J. W. Pan, Genuine High-Order Einstein-Podolsky-Rosen Steering, Phys. Rev. Lett. **115**, 010402 (2015).
[19] Q. Y. He, L. Rosales-Zárate, G. Adesso, and M. D. Reid, Secure Continuous Variable Teleportation and Einstein–Podolsky–Rosen Steering, Phys. Rev. Lett. **115**, 180502 (2015).
[20] M. D. Reid, Signifying quantum benchmarks for qubit teleportation and secure quantum communication using Einstein–Podolsky–Rosen steering inequalities, Phys. Rev. A **88**, 062338 (2013).
[21] C. Y. Chiu, N. Lambert, T. L. Liao, F. Nori, and C. M. Li, No-cloning of quantum steering, npj Quantum Inf. **2**, 16020 (2016).
[22] M. Piani and J. Watrous, Necessary and Sufficient Quantum Information Characterization of Einstein–Podolsky–Rosen Steering, Phys. Rev. Lett. **114**, 060404 (2015).
[23] C. H. Bai, D. Y. Wang, S. Zhang, S. Liu, and H. F. Wang, Strong mechanical squeezing in a standard optomechanical system by pump modulation, Phys. Rev. A **101**, 053836 (2020).
[24] C. Kittel, On the theory of ferromagnetic resonance absorption, Phys. Rev. **73**, 155 (1948).
[25] H. Huebl, C. W. Zollitsch, J. Lotze, F. Hocke, M. Greifenstein, A. Marx, R. Gross, and S. T. B. Goennenwein, High Cooperativity in Coupled Microwave Resonator Ferrimagnetic Insulator Hybrids, Phys. Rev. Lett. **111**, 127003 (2013).
[26] Y. Tabuchi, S. Ishino, T. Ishikawa, R. Yamazaki, K. Usami, and Y. Nakamura, Hybridizing Ferromagnetic Magnons and Microwave Photons in the Quantum Limit, Phys. Rev. Lett. **113**, 083603 (2014).
[27] X. Zhang, C. L. Zou, L. Jiang, and H. X. Tang, Strongly Coupled Magnons and Cavity Microwave Photons, Phys. Rev. Lett. **113**, 156401 (2014).
[28] M. Goryachev, W. G. Farr, D. L. Creedon, Y. Fan, M. Kostylev, and M. E. Tobar, High-Cooperativity Cavity QED with Magnons at Microwave Frequencies, Phys. Rev. Appl. **2**, 054002 (2014).
[29] L. Bai, M. Harder, Y. P. Chen, X. Fan, J. Q. Xiao, and C. M. Hu, Spin Pumping in Electrodynamically Coupled Magnon-Photon Systems, Phys. Rev. Lett. **114**, 227201 (2015).
[30] D. Zhang, X. Q. Luo, Y. P. Wang, T. F. Li, and J. Q. You, Observation of the exceptional point in cavity magnon-polaritons, Nat. Commun. **8**, 1368 (2017).
[31] L. H. Bai, M. Harder, P. Hyde, Z. H. Zhang, C. M. Hu, Y. P. Chen, and J. Q. Xiao, Cavity Mediated Manipulation of Distant Spin Currents Using a Cavity-Magnon-Polariton, Phys. Rev. Lett. **118**, 217201 (2017).
[32] Y. P. Wang, G. Q. Zhang, D. K. Zhang, T. F. Li, C. M. Hu, and J. Q. You, Bistability of Cavity Magnon Polaritons, Phys. Rev. Lett. **120**, 057202 (2018).
[33] Y. Tabuchi, S. Ishino, A. Noguchi, T. Ishikawa, R. Yamazaki, K. Usami, and Y. Nakamura, Coherent coupling between a ferromagnetic magnon and a superconducting qubit, Science **349**, 405 (2015).
[34] D. Lachance-Quirion, Y. Tabuchi, S. Ishino, A. Noguchi, T. Ishikawa, R. Yamazaki, and Y. Nakamura, Resolving quanta of collective spin excitations in a millimeter-sized ferromagnet, Sci. Adv. **3**, e1603150 (2017).
[35] X. F. Zhang, C. L. Zou, L. Jiang, and H. X. Tang, Cavity magnomechanics, Sci. Adv. **2**, e1501286 (2016).
[36] X. F. Zhang, N. Zhu, C. L. Zou, and H. X. Tang, Optomagnonic Whispering Gallery Microresonators, Phys. Rev. Lett. **117**, 123605 (2016).
[37] A. Osada, R. Hisatomi, A. Noguchi, Y. Tabuchi, R. Yamazaki, K. Usami, M. Sadgrove, R. Yalla, M. Nomura, and Y. Nakamura, Cavity Optomagnonics with Spin-Orbit Coupled Photons, Phys. Rev. Lett. **116**, 223601 (2016).
[38] S. Sharma, Y. M. Blanter, and G. E. W. Bauer, Optical Cooling of Magnons, Phys. Rev. Lett. **121**, 087205 (2018).
[39] J. Li, S. Y. Zhu, and G. S. Agarwal, Magnon-Photon-Phonon Entanglement in Cavity Magnomechanics, Phys. Rev. Lett. **121**, 203601 (2018).
[40] J. Li, S. Y. Zhu, and G. S. Agarwal, Squeezed states of magnons and phonons in cavity magnomechanics, Phys. Rev. A **99**, 021801(R) (2019).
[41] C. Kong, H. Xiong, and Y. Wu, Magnon-Induced Nonreciprocity Based on the Magnon Kerr Effect, Phys. Rev. Appl. **12**, 034001 (2019).
[42] J. M. P. Nair and G. S. Agarwal, Deterministic quantum entanglement between macroscopic ferrite samples, Appl. Phys. Lett. **117**, 084001 (2020).
[43] Z. D. Zhang, M. O. Scully, and G. S. Agarwal, Quantum entanglement between two magnon modes via Kerr nonlinearity driven far from equilibrium, Phys. Rev. Res. **1**, 023021 (2019).
[44] H. Y. Yuan, P. Yan, S. S. Zheng, Q. Y. He, K. Xia, and M. H. Yung, Steady Bell State Generation via Magnon-Photon Coupling, Phys. Rev. Lett. **124**, 053602 (2020).
[45] Y. P. Wang, J. W. Rao, Y. Yang, P. C. Xu, Y. S. Gui, B. M. Yao, J. Q. You, and C. M. Hu, Nonreciprocity and

Unidirectional Invisibility in Cavity Magnonics, Phys. Rev. Lett. **123**, 127202 (2019).
[46] J. Li and S. Y. Zhu, Entangling two magnon modes via magnetostrictive interaction, New J. Phys. **21**, 085001 (2019).
[47] P. C. Xu, J. W. Rao, Y. S. Gui, X. F. Jin, and C. M. Hu, Cavity-mediated dissipative coupling of distant magnetic moments: Theory and experiment, Phys. Rev. B **100**, 094415 (2019).
[48] D. Lachance-Quirion, Y. Tabuchi, A. Gloppe, K. Usami, and Y. Nakamura, Hybrid quantum systems based on magnonics, Appl. Phys. Exp. **12**, 070101 (2019).
[49] C. M. Hu, Chapter four – the 2020 roadmap for spin cavitronics, Solid State Phys. **71**, 117 (2020).
[50] E. Almpanis, *Optomagnonic Structures* (NCSR "Demokritos", Greece & National and Kapodistrian University of Athens, Greece, 2020).
[51] P. A. Fleury, S. P. S. Porto, L. E. Cheesman, and H. J. Guggenheim, Light Scattering by Spin Waves in FeF_2, Phys. Rev. Lett. **17**, 84 (1966).
[52] H. L. Hu and F. R. Morgenthaler, Strong infrared-light scattering from coherent spin waves in yttrium iron garnet, Appl. Phys. Lett. **18**, 307 (1971).
[53] J. R. Sandercock and W. Wettling, Light scattering from thermal magnons in iron and nickel, IEEE Trans. Magn. **14**, 442 (1978).
[54] S. O. Demokritov, V. E. Demidov, O. Dzyapko, G. A. Melkov, A. A. Serga, B. Hillebrands, and A. N. Slavin, Bose–Einstein condensation of quasi-equilibrium magnons at room temperature under pumping, Nature **443**, 430 (2006).
[55] A. A. Serga, V. S. Tiberkevich, C. W. Sandweg, V. I. Vasyuchka, D. A. Bozhko, A. V. Chumak, T. Neumann, B. Obry, G. A. Melkov, A. N. Slavin, and B. Hillebrands, Bose–Einstein condensation in an ultra-hot gas of pumped magnons, Nat. Commun. **5**, 3452 (2014).
[56] J. A. Haigh, A. Nunnenkamp, A. J. Ramsay, and A. J. Ferguson, Triple-Resonant Brillouin Light Scattering in Magneto-Optical Cavities, Phys. Rev. Lett. **117**, 133602 (2016).
[57] B. Z. Rameshti and G. E. W. Bauer, Indirect coupling of magnons by cavity photons, Phys. Rev. B **97**, 014419 (2018).
[58] G. Q. Zhang and J. Q. You, Higher-order exceptional point in a cavity magnonics system, Phys. Rev. B **99**, 054404 (2019).
[59] See Supplemental Material at http://link.aps.org/supplemental/10.1103/PhysRevApplied.15.024042 for a discussion of some nonlinear terms, derivation of the diffusion matrix, stability conditions of system, etc.
[60] B. Yurke, Squeezed-state generation using a Josephson parametric amplifier, J. Opt. Soc. Am. B **4**, 1551 (1987).
[61] B. Yurke, P. G. Kaminsky, R. E. Miller, E. A. Whittaker, A. D. Smith, A. H. Silver, and R. W. Simon, Observation of 4.2-K Equilibrium-Noise Squeezing via a Josephson-Parametric Amplifier, Phys. Rev. Lett. **60**, 764 (1988).
[62] B. Yurke, L. R. Corruccini, P. G. Kaminsky, L. W. Rupp, A. D. Smith, A. H. Silver, R. W. Simon, and E. A. Whittaker, Observation of parametric amplification and deamplification in a Josephson parametric amplifier, Phys. Rev. A **39**, 2519 (1989).
[63] R. Movshovich, B. Yurke, P. G. Kaminsky, A. D. Smith, A. H. Silver, R. W. Simon, and M. V. Schneider, Observation of Zero-Point Noise Squeezing via a Josephson-Parametric Amplifier, Phys. Rev. Lett. **65**, 1419 (1990).
[64] M. A. Castellanos-Beltran, K. D. Irwin, G. C. Hilton, L. R. Vale, and K. W. Lehnert, Amplification and squeezing of quantum noise with a tunable Josephson metamaterial, Nat. Phys. **4**, 929 (2008).
[65] T. Yamamoto, K. Inomata, M. Watanabe, K. Matsuba, T. Miyazaki, W. D. Oliver, Y. Nakamura, and J. S. Tsai, Flux-driven Josephson parametric amplifier, Appl. Phys. Lett. **93**, 042510 (2008).
[66] F. Mallet, M. A. Castellanos-Beltran, H. S. Ku, S. Glancy, E. Knill, K. D. Irwin, G. C. Hilton, L. R. Vale, and K. W. Lehnert, Quantum State Tomography of an Itinerant Squeezed Microwave Field, Phys. Rev. Lett. **106**, 220502 (2011).
[67] E. P. Menzel, R. Di Candia, F. Deppe, P. Eder, L. Zhong, M. Ihmig, M. Haeberlein, A. Baust, E. Hoffmann, D. Ballester, K. Inomata, T. Yamamoto, Y. Nakamura, E. Solano, A. Marx, and R. Gross, Path Entanglement of Continuous-Variable Quantum Microwaves, Phys. Rev. Lett. **109**, 250502 (2012).
[68] L. Zhong, E. P. Menzel, R. D. Candia, P. Eder, M. Ihmig, A. Baust, M. Haeberlein, E. Hoffmann, K. Inomata, T. Yamamoto, Y. Nakamura, E. Solano, F. Deppe, A. Marx, and R. Gross, Squeezing with a flux-driven Josephson parametric amplifier, New J. Phys. **15**, 125013 (2013).
[69] K. G. Fedorov, L. Zhong, S. Pogorzalek, P. Eder, M. Fischer, J. Goetz, E. Xie, F. Wulschner, K. Inomata, T. Yamamoto, Y. Nakamura, R. Di Candia, U. Las Heras, M. Sanz, E. Solano, E. P. Menzel, F. Deppe, A. Marx, and R. Gross, Displacement of Propagating Squeezed Microwave States, Phys. Rev. Lett. **117**, 020502 (2016).
[70] S. Kono, Y. Masuyama, T. Ishikawa, Y. Tabuchi, R. Yamazaki, K. Usami, K. Koshino, and Y. Nakamura, Nonclassical Photon Number Distribution in a Superconducting Cavity under a Squeezed Drive, Phys. Rev. Lett. **119**, 023602 (2017).
[71] A. Bienfait, P. Campagne-Ibarcq, A. H. Kiilerich, X. Zhou, S. Probst, J. J. Pla, T. Schenkel, D. Vion, D. Esteve, J. J. L. Morton, K. Moelmer, and P. Bertet, Magnetic Resonance with Squeezed Microwaves, Phys. Rev. X **7**, 041011 (2017).
[72] M. Malnou, D. A. Palken, Leila R. Vale, Gene C. Hilton, and K. W. Lehnert, Optimal Operation of a Josephson Parametric Amplifier for Vacuum Squeezing, Phys. Rev. Appl. **9**, 044023 (2018).
[73] C. W. Gardiner, Inhibition of Atomic Phase Decays by Squeezed Light: A Direct Effect of Squeezing, Phys. Rev. Lett. **56**, 1917 (1986).
[74] D. Vitali, S. Gigan, A. Ferreira, H. R. Bohm, P. Tombesi, A. Guerreiro, V. Vedral, A. Zeilinger, and M. Aspelmeyer, Optomechanical Entanglement between a Movable Mirror and a Cavity Field, Phys. Rev. Lett. **98**, 030405 (2007).
[75] I. Kogias, A. R. Lee, S. Ragy, and G. Adesso, Quantification of Gaussian Quantum Steering, Phys. Rev. Lett. **114**, 060403 (2015).
[76] G. Vidal and R. F. Werner, Computable measure of entanglement, Phys. Rev. A **65**, 032314 (2002).

[77] G. Adesso, A. Serafini, and F. Illuminati, Extremal entanglement and mixedness in continuous variable systems, Phys. Rev. A **70**, 022318 (2004).

[78] J. Eisert, Ph.D. thesis, University of Potsdam, Potsdam, 2001.

[79] M. B. Plenio, Logarithmic Negativity: A Full Entanglement Monotone That is not Convex, Phys. Rev. Lett. **95**, 090503 (2005).

[80] C. G. Liao, H. Xie, R. X. Chen, M. Y. Ye, and X. M. Lin, Controlling one-way quantum steering in a modulated optomechanical system, Phys. Rev. A **101**, 032120 (2020).

[81] E. X. DeJesus and C. Kaufman, Routh–Hurwitz criterion in the examination of eigenvalues of a system of nonlinear ordinary differential equations, Phys. Rev. A **35**, 5288 (1987).

[82] I. Boventer, M. Pfirrmann, J. Krause, Y. Schön, M. Kläui, and M. Weides, Complex temperature dependence of coupling and dissipation of cavity magnon polaritons from millikelvin to room temperature, Phys. Rev. B **97**, 184420 (2018).

[83] R. Gross and A. Marx, *Festkörperphysik* (Oldenbourg Wissensch. Vlg, Munich, 2012).

[84] The relation between static field $\mathbf{H} = (0, 0, H_z)$ in one direction and resonant frequency $\omega_{1,2}$, with demagnetizing factors N_i $[i = (x, y, z)]$, is given by $\omega_{1,2} = \gamma_0\sqrt{[H_z + (N_y - N_z)M_z][H_z + (N_x - N_z)M_z]}$ with M_z representing saturation magnetization. For a sphere $N_x = N_y = N_z = \frac{4}{3}\pi$ and the dispersion relation reads $\omega_{1,2} = \gamma_0 H_z$ [24].

[85] D. Zhang, X. M. Wang, T. F. Li, X. Q. Luo, W. Wu, F. Nori, and J. Q. You, Cavity quantum electrodynamics with ferromagnetic magnons in a small yttrium-iron-garnet sphere, npj Quantum Inf. **1**, 15014 (2015).

[86] X. F. Zhang, C. L. Zou, N. Zhu, F. Marquardt, L. Jiang, and H. X. Tang, Magnon dark modes and gradient memory, Nat. Commun. **6**, 8914 (2015).

[87] T. A. Palomaki, J. D. Teufel, R. W. Simmonds, and K. W. Lehnert, Entangling mechanical motion with microwave fields, Science **342**, 710 (2013).

[88] D. M. Pozar, *Microwave Engineering* (John Wiley & Sons, New York, 2011).

[89] J. Walowski, M. Münzenberg, Perspective: Ultrafast magnetism and THz spintronics, J. Appl. Phys. **120**, 140901 (2016).

[90] N. Maccaferri, I. Zubritskaya, I. Razdolski, I. A. Chioar, V. Belotelov, V. Kapaklis, P. M. Oppeneer, and A. Dmitriev, Nanoscale magnetophotonics, J. Appl. Phys. **127**, 080903 (2020).

[91] J. Walowski, G. Müller, M. Djordjevic, M. Münzenberg, M. Kläui, C. A. F. Vaz, and J. A. C. Bland, Energy Equilibration Processes of Electrons, Magnons, and Phonons at the Femtosecond Time Scale, Phys. Rev. Lett. **101**, 237401 (2008).

[92] S. Schlauderer, C. Lange, S. Baierl, T. Ebnet, C. P. Schmid, D. C. Valovcin, A. K. Zvezdin, A. V. Kimel, R. V. Mikhaylovskiy, and R. Huber, Temporal and spectral fingerprints of ultrafast all-coherent spin switching, Nature **569**, 383 (2019).